PNAS RESEARCH ARTICLE | ENGINEERING
APPLIED BIOLOGICAL SCIENCES

Silver electroceutical technology to treat sarcopenia

Min Young Kim[a], Hyun Young Shin[b,c], Sung Chun Cho[d], Sohae Yang[a], Aseer Intisar[a], Hyeong Jung Woo[a], Youn-Suk Choi[e], Chang-Lim You[f], Jong-Sun Kang[f], Yun-Il Lee[d], Sang Chul Park[g], Kyungmoo Yea[a], Tae Gyu Oh[h], Michael Downes[h], Ronald M. Evans[h], and Minseok S. Kim[a,b,i,j,1]

Edited by Luke P. Lee, Harvard Medical School, Boston, MA; received January 2, 2023; accepted June 22, 2023 by Editorial Board Member John A. Rogers

While the world is rapidly transforming into a superaging society, pharmaceutical approaches to treat sarcopenia have hitherto not been successful due to their insufficient efficacy and failure to specifically target skeletal muscle cells (skMCs). Although electrical stimulation (ES) is emerging as an alternative intervention, its efficacy toward treating sarcopenia remains unexplored. In this study, we demonstrate a silver electroceutical technology with the potential to treat sarcopenia. First, we developed a high-throughput ES screening platform that can simultaneously stimulate 15 independent conditions, while utilizing only a small number of human-derived primary aged/young skMCs (hAskMC/hYskMC). The in vitro screening showed that specific ES conditions induced hypertrophy and rejuvenation in hAskMCs, and the optimal ES frequency in hAskMCs was different from that in hYskMCs. When applied to aged mice in vivo, specific ES conditions improved the prevalence and thickness of Type IIA fibers, along with biomechanical attributes, toward a younger skMC phenotype. This study is expected to pave the way toward an electroceutical treatment for sarcopenia with minimal side effects and help realize personalized bioelectronic medicine.

integrated electrical stimulation biochip | multiplex screening technology | electroceutical | sarcopenia | personalized electric medicine

Significance

Electrical stimulation (ES) treatment showed beneficial effects in recovering skeletal muscle in in vivo and in vitro. Therefore, many clinical studies tried to treat sarcopenia but did not show adequate rehabilitation effects. Here, we elucidate that specific ES conditions are required to recover young and aged skeletal muscle, respectively. According to the specific ES condition, our results show that calcium signaling, senescence, metabolism, and hypertrophic effects are recovered via specific ES conditions. However, suboptimal ES conditions induced muscle damage. In addition, applying specific ES conditions to the aged mice induces hypertrophy and restores contraction force. Consequently, the optimal ES condition we named "silver electroceutical" can be an alternative to treat sarcopenia.

Sarcopenia is an age-related skeletal muscle disorder that causes an accelerated loss of muscle mass and function, which can lead to a decline in mobility, injury due to falls, and mortality (1–3). Despite numerous attempts to treat sarcopenia via biochemical drugs, no medication is currently available (4). For example, targeting the myostatin pathway has been extensively investigated (5–7). However, myostatin inhibition causes severe side effects such as cardiac disorders, basal and squamous cell carcinomas, telangiectasia, and erythema (8, 9). Although myostatin inhibition can lead to an increase in muscle mass, it is not accompanied by an increase in force generation (10). Therefore, this approach has not been approved for treating sarcopenia. Bimagrumab is another drug that has been tested to treat muscle loss and weakness but was proven to be ineffective in treating sarcopenia in a randomized clinical trial (9). Other pharmacological approaches for the treatment of sarcopenia include AMPK agonists and anabolic hormones, which also lead to adverse side effects, including neurodegeneration, nerve damage, and edema. Consequently, pharmacological approaches have not been successful, owing to their severe side effects and insufficient efficacy.

Currently, the only option for managing the symptoms of sarcopenia is physical exercise (11, 12). However, this might not be a practical option for the geriatric population because of their physical frailty. In addition, prolonged suppression of physical activity during the COVID-19 pandemic has exacerbated sarcopenia (13, 14). Therefore, it is critical to explore an effective and practical therapeutic solution that can specifically target the skeletal muscles to treat sarcopenia with minimal side effects (15, 16).

The key investigations of this study were to find out whether the electroceutical approach has the potential to treat sarcopenia and the optimal stimulation condition for the intervention. ES has shown various beneficial effects in normal skeletal muscle cells (skMC), such as the prevention of insulin resistance, maturation of skeletal muscle, and enhancement of sarcomere assembly (17–20). Although extensive ES research has been reported, systematic studies on the efficacy of ES are insufficient because the results are generated with different stimulation conditions and ES devices, which usually stimulate skMC under a nonuniform E-field (Electric field). In addition, most studies that investigated the effects of ES on skMC have used rodent-derived skMCs such as C2C12, which do not exhibit the characteristics of senescent cells such as human-derived primary aged skMC (hAskMC) (18, 20–26). As no study has reported the effect of ES in hAskMC, the systematic investigation of ES as a treatment for sarcopenia has remained unexplored (17, 19). Therefore, it is necessary to conduct a systematic investigation of diverse ES conditions via high-throughput screening (HTS) to identify the optimal ES parameter that can ameliorate the critical features of sarcopenia in human-derived primary young skMCs (hYskMC). However, most ES devices

Author contributions: M.Y.K., H.Y.S., S.C.P., and M.S.K. designed research; M.Y.K., H.Y.S., S.C.C., S.Y., Y.-S.C., and M.S.K. performed research; M.Y.K., Y.-I.L., and M.S.K. contributed new reagents/analytic tools; M.Y.K., H.J.W., C.-L.Y., J.-S.K., Y.-I.L., S.C.P., K.Y., T.G.O., M.D., R.M.E., and M.S.K. analyzed data; and M.Y.K., A.I., and M.S.K. wrote the paper.

The authors declare no competing interest.

This article is a PNAS Direct Submission. L.P.L. is a guest editor invited by the Editorial Board.

Copyright © 2023 the Author(s). Published by PNAS. This article is distributed under Creative Commons Attribution-NonCommercial-NoDerivatives License 4.0 (CC BY-NC-ND).

[1]To whom correspondence may be addressed. Email: kms@dgist.ac.kr.

This article contains supporting information online at https://www.pnas.org/lookup/suppl/doi:10.1073/pnas.2300036120/-/DCSupplemental.

Published August 7, 2023.

utilized for skMC are incompatible with the HTS format and typically require a large number of cells (27). Considering the cost and limited source of hAskMC, it is crucial to develop a suitable ES screening platform that enables high-throughput ES screening (HiTESS) using a small number of cells.

In this study, we introduce a silver electroceutical technology to treat sarcopenia with minimal side effects. First, we developed a HiTESS platform that can simultaneously stimulate 15 independent conditions with a highly uniform E-field and also perform multiplex screening using a small quantity of hAskMC (~3,000 cells/chamber). We utilized skMC from 17-y-old and 68-y-old male donors as hYskMC and hAskMC, respectively. In vitro screening showed that specific ES conditions were effective at recovering senescence and inducing hypertrophic characteristics in hAskMCs (Fig. 1). Interestingly, the optimal ES conditions for the most significant improvements were 50 and 500 Hz for the hYskMC and hAskMCs, respectively. Subsequently, we carried out a preclinical study by applying ES in vivo five times per week for six consecutive weeks. In aged mice, the optimized ES (500 Hz) led to significant improvements in the prevalence and thickness of Type IIA fibers, as well as twitch and tetanus force generation, bringing these characteristics closer to the levels observed in young mice. Finally, RNA sequencing showed that ES resulted in the recuperation of gene expression in hAskMC, particularly in genes related to myogenesis, myofiber differentiation, and nervous system development. Based on these results, this study demonstrates that an electroceutical approach has the potential to offer an alternative intervention for treating sarcopenia. Meanwhile, the age-dependent efficacy of the ES condition will help to realize the era of personalized bioelectronic medicine.

Results

HiTESS Platform with Uniform E-Field. The HiTESS assembly is configured with six components: the bottom holder, HiTESS substrate, chamber with an O-ring, connecting PCB, upper holder, and chamber cover (Fig. 2*A*), and each component is assembled according to the sequence shown in *SI Appendix*, Fig. S1 *A* and *B*. The HiTESS substrate was designed so that its function required a minimal number of skMCs. Therefore, we created a 2 × 2 mm well containing 3,000 cells (28), which was 13-fold lower than the number of cells required per well in a 96-well plate (Fig. 2*B*). Moreover, the HiTESS assembly is simply connected to the HiTESS pulse generator (Fig. 2*C*), which can simultaneously generate 15 different electrical pulses controlled using custom-made software (Fig. 2*C* and *SI Appendix*, Fig. S1*C*). The electrical pulse from the HiTESS pulse generator is transmitted to the HiTESS substrate through the connecting PCB and pogo pins (Fig. 2*D*). Each channel of the HiTESS pulse generator can generate pulse stimulation conditions with voltage ranging from −10 to +10 V, frequency ranging from 0.01 to 50 kHz, and pulse widths ranging from 2.5 μs to 160 s (*SI Appendix*, Table S1).

We performed COMSOL Multiphysics simulation to optimize the electrode dimensions that can generate a highly uniform E-field as well as a low electric current density in the individual culture well of the HiTESS substrate. To optimize the distance between electrodes, simulations were performed with the electrode distance ranging from 3 to 5 mm with 0.5 mm intervals (fixed parameters: width 0.2 mm, length 4 mm, and medium height 5 mm) (*SI Appendix*, Fig. S2 *A*

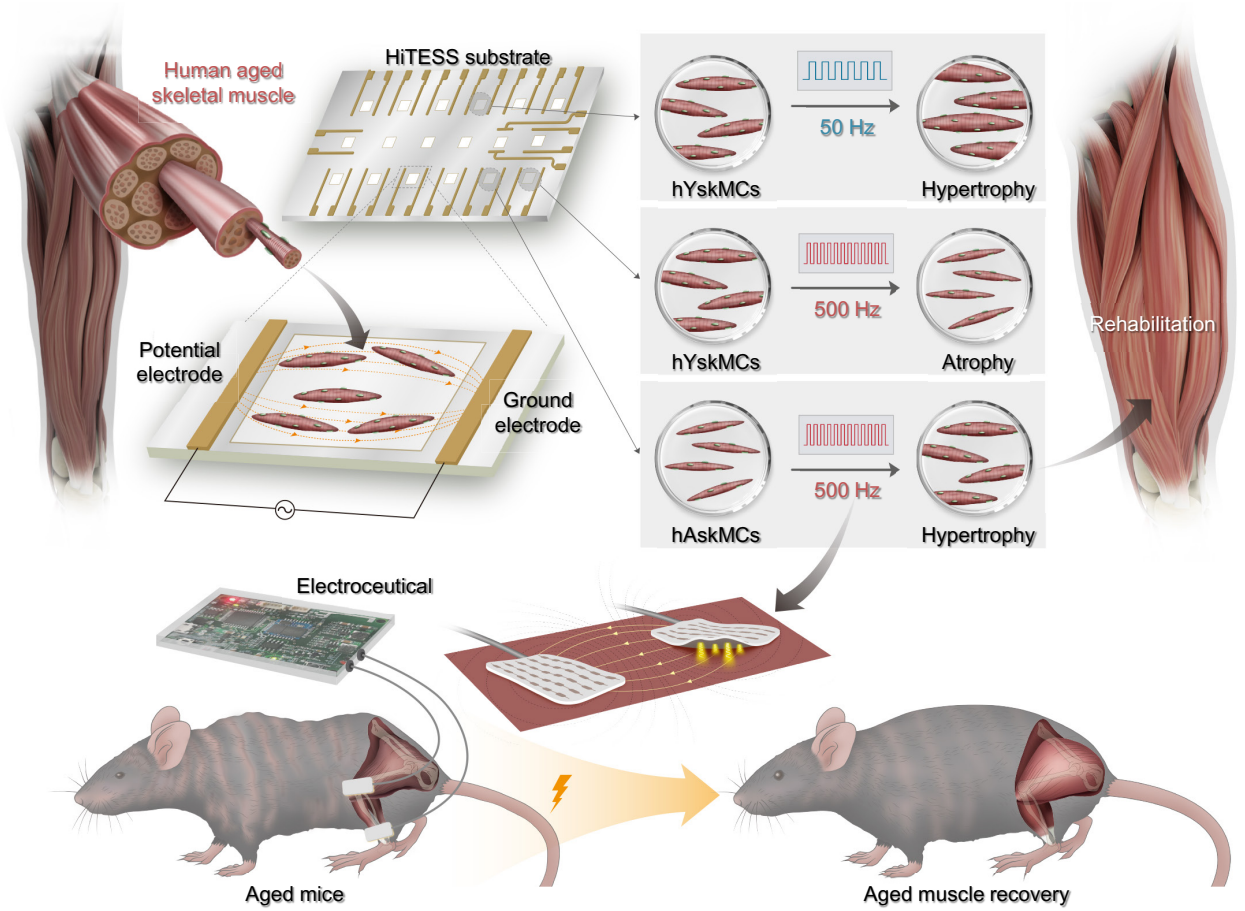

Fig. 1. Schematic of the silver electroceutical to restore the aged skeletal muscle into a young-phenotypic muscle. Skeletal muscle responds differently depending on ES conditions, and identical ES conditions result in different cell fates depending on young and aged skeletal muscles.

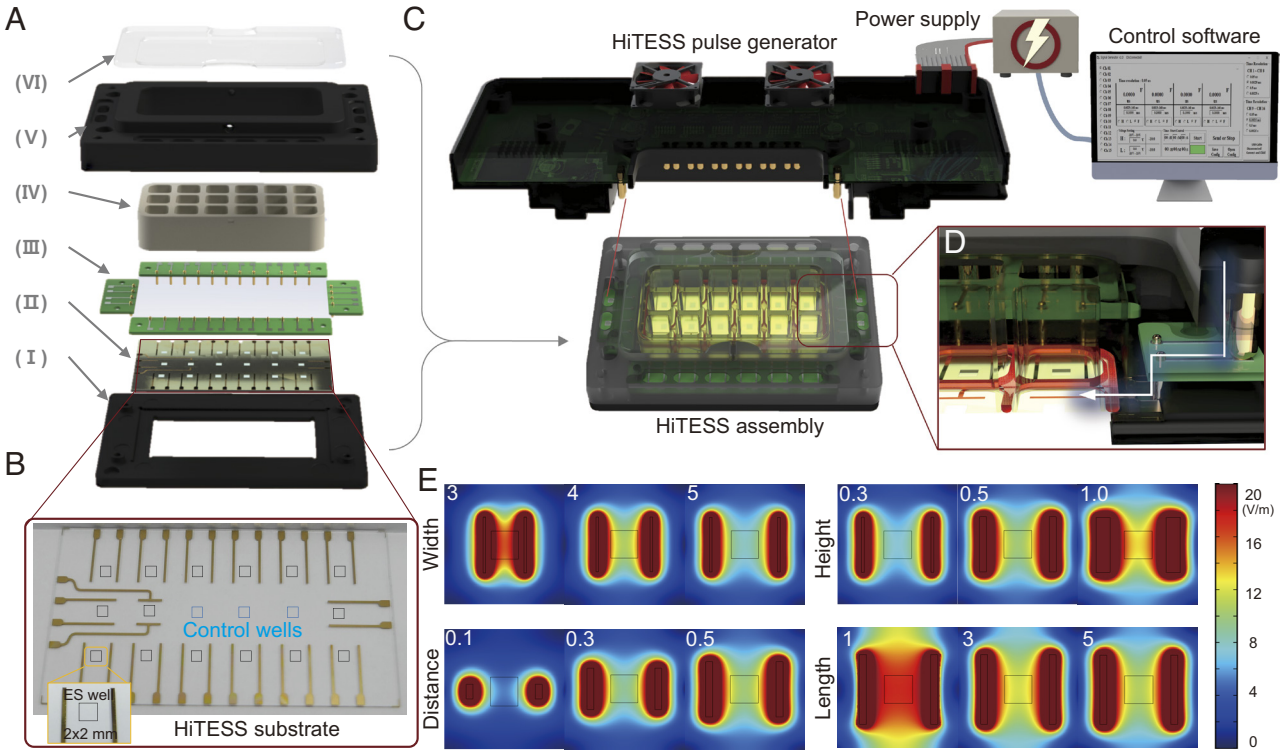

Fig. 2. Configuration of the HiTESS platform and simulation for electric field optimization. (*A*) Configuration of the high-throughput electrical stimulation screening (HiTESS) assembly. (I) Bottom holder, (II) HiTESS substrate, (III) connecting PCB, (IV) chamber with O-ring, (V) upper holder, and (VI) cover. (*B*) Plane view of the HiTESS substrate. The black (ES) and blue (no ES) boxes indicate the individual culture well. (*C*) HiTESS assembly connected with HiTESS pulse generator. The HiTESS pulse generator was controlled by custom-made control software. (*D*) HiTESS assembly and HiTESS pulse generator are connected through the contact between the connecting PCB and the pogo pins of the pulse generator. (*E*) Simulation results of E- fields based on distance, width, length, and medium height.

and *B*). The E-field uniformity increased with increasing distance between the electrodes, whereas the E-field, current density, and total current decreased (Fig. 2*E* and *SI Appendix,* Fig. S3 *A and E*). Therefore, a 5 mm electrode distance was selected because it generated the highest uniformity while maintaining the lowest current density and total current. To optimize the electrode width, we performed the simulation for width ranging from 0.2 to 1.0 mm with 0.1 mm intervals (fixed parameters: electrode distance 5.0 mm, length 4 mm, and medium height 5 mm). The results indicated that while the E-field and total current increased as the electrode width increased, the uniformity and current density decreased. Therefore, to obtain a balanced condition of adequate E-field uniformity and minimal risk of electrolysis, 0.5 mm electrode width was selected (Fig. 2*E* and *SI Appendix,* Fig. S3 *B and F*). Subsequently, simulation was conducted for electrode length of 1.0 to 5.0 mm with 1 mm intervals (fixed parameters: electrode distance 5.0 mm, width 0.5 mm, and medium height 5 mm). According to the results, the E-field uniformity and total current increased with increasing electrode length, whereas the current density decreased (Fig. 2*E* and *SI Appendix,* Fig. S3 *C and G*). Thus, an electrode length of 5 mm was selected, as it provides the highest E-field uniformity and the lowest current density. Finally, after optimizing the electrode dimensions, a simulation was performed for the height of the culture medium ranging from 1 to 10 mm with 1 mm intervals. As the medium height increased, the E-field, uniformity, and total current decreased; however, the current density exhibited an inverse tendency. When the E-field uniformity and current density were considered, the 5 mm height of the culture medium was optimal because the extent of changes beyond a height of 5 mm was negligible (Fig. 2*E* and *SI Appendix,* Fig. S3 *D and H*). Based on the optimization process via simulation, the electrode dimensions were determined as 0.5 mm width, length as 5 mm, and distance as 5 mm, and the final E-field uniformity reflecting the dimensions was 95% with an electrode surface current density of 105 A/m^2 and a total current of 64 μA.

To prevent heat generated by the stimulator, we installed four cooling fans in the HiTESS platform. Additionally, we used a thermal imaging camera to measure the temperature of the HiTESS platform, culture chamber, and substrate bottom to verify whether there was any heat generation due to all ES conditions. The results showed that there was no significant temperature rise (< 1 °C) during ES (*SI Appendix*, Fig. S4).

The Optimal ES Condition for Inducing Hypertrophy and Myogenesis Is Different in hYskMC and hAskMC. To identify the conditions that induce hypertrophy, we first screened the E-field ranging from 11.5 to 57.6 V/m (frequency fixed at 50 Hz). The thicknesses of ten myotubes were measured to evaluate the hypertrophic effect of ES in each culture well. The results showed that, while the myotube diameter increased at 11.5 V/m in both hYskMC and hAskMC, it decreased beyond 23 V/m (*SI Appendix*, Fig. S8). Thus, the E-field was determined as 11.5 V/m. Subsequently, we performed ES screening depending on the frequency (0.1 to 10 kHz) at a fixed 11.5 V/m E-field. The results showed that within the frequency range of 0.1 to 50 Hz, the myotube diameter gradually increased in both hYskMC and hAskMC (Fig. 3*A* and *SI Appendix,* Fig. S9). Interestingly, however, the two groups exhibited opposite responses at 500 Hz: hYskMC exhibited narrower myofibers, while hAskMC exhibited maximal efficacy in terms of hypertrophy (Fig. 3 *A* and *B*). Meanwhile, ES beyond 500 Hz led to atrophy in both hYskMC and hAskMC. Therefore, the most effective ES frequency to increase the myotube diameter was 50 Hz for hYskMC and 500 Hz for hAskMC, indicating that the optimal ES frequency varies with age.

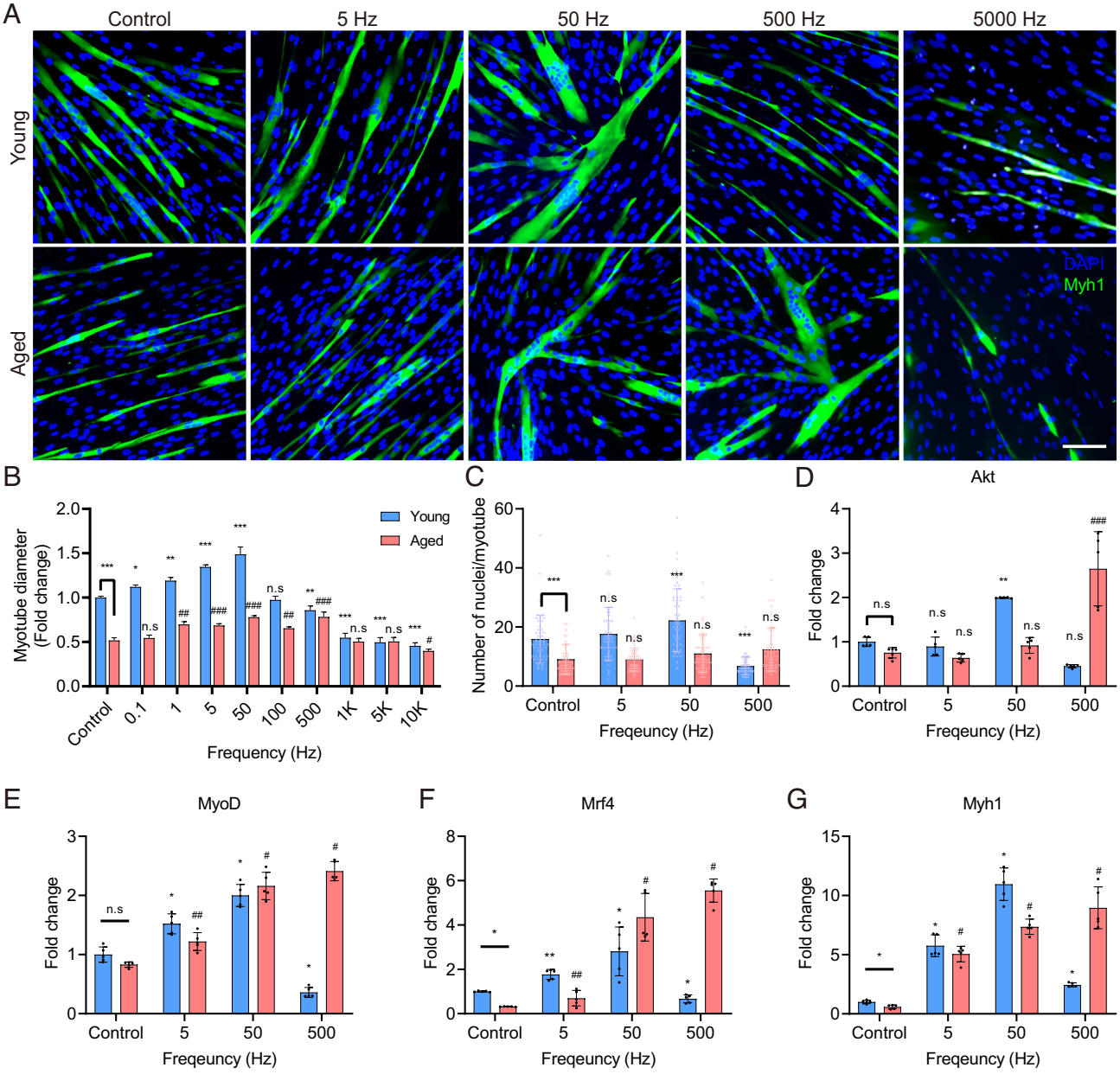

Fig. 3. Specific ES conditions induce myotube differentiation. (*A* and *B*) Representative images (*A*) and quantification (*B*) of myotubes stained with Myh1 and nuclei, respectively. Optimal ES frequencies vary with age. (Scale bar, 100 μm.) (*C*) Quantification of the number of nuclei/myotube. The optimal ES frequency for hYskMC and hAskMC is 50 and 500 Hz, respectively. (*D*–*G*) mRNA expression levels of Akt (*D*), MyoD (*E*), Mrf4 (*F*), and Myh1 (*G*). The gene expression profiles are up-regulated at the appropriate ES condition. (*$P < 0.05$; **$P < 0.01$; ***$P < 0.001$; compared to young control, $^{\#}P < 0.05$; $^{\#\#}P < 0.01$; $^{\#\#\#}P < 0.001$; compared to aged control).

Further analysis was conducted to count the number of nuclei/myotube (Fig. 3*C*), which is one of the most fundamental indicators in myotube analysis. As several myoblasts fuse to form a single myotube, a higher number of nuclei/myotube corresponds to a greater degree of myoblast fusion (29). While the average number of nuclei/myotube showed a tendency to increase at 5 and 50 Hz, it significantly decreased at 500 Hz in hYskMC. Although it did not show statistical significance depending on the three frequencies in hAskMC, the average number of nuclei/myotube gradually increased in hAskMC until the ES frequency reached 500 Hz. The number of nuclei/myotube analysis showed a similar trend with the myotube diameter. The data further supported that the optimal ES frequencies for hYskMC and hAskMC were 50 and 500 Hz, respectively.

Subsequently, to verify the changes in myotube diameter and number of nuclei/myotube changes depending on ES, we investigated the mRNA expression levels related to myogenesis using four specific genes Akt, which induces protein synthesis and division in muscle (Fig. 3*D*); MyoD and Mrf4, which are both master regulatory factors of myogenesis (Fig. 3 *E* and *F*); and Myh1, which encodes the myosin heavy chain I protein forming myotubes (Fig. 3*G*). Remarkably, depending on the frequencies, all the gene expression profiles showed a similar tendency with the myotube differentiation and number of nuclei/myotube results: the greatest degree of upregulation for the four genes in hYskMC and hAskMC occurred at 50 and 500 Hz, respectively. At 500 Hz, in the hAskMC, the expression of Akt increased by 2.7-fold, MyoD by 2.4-fold, Mrf4 by 5.5-fold, and Myh1 by 9.0-fold, respectively. Gene ontology (GO) analyses were performed to gain a deeper understanding of the functional improvement of hAskMC. The results showed that six GO terms were commonly up-regulated in young versus aged and aged 500 Hz

versus aged control, including muscle structure development, muscle cell differentiation, muscle tissue development, muscle organ development, muscle adaptation, and regulation of muscle system process (*SI Appendix,* Fig. S10 *A* and *B*). Furthermore, we verified the consistency of the hypertrophy effect in different donors (20- and 66-y-old males, 20M & 66M) via evaluating the myotube diameter as well as Myh1, MyoG, Mef2 gene expression (*SI Appendix,* Fig. S11). In 20M, as in hYskMC, we observed hypertrophy at 5 and 50 Hz, whereas at 500 Hz, we observed atrophy. Meanwhile, in 66M, we observed that hypertrophy was induced at 5, 50, and 500 Hz. From the results, we inferred that not all ES positively affects the hYskMC and hAskMC, and the hAskMC can recover to young-like skeletal muscle phenotypes via the specific ES condition. In addition, the response to ES conditions differs depending on the age, and the optimal ES frequency to induce hypertrophy and myogenesis in hYskMC and hAskMC is different.

The Potential of the Specific ES to Recover Senescence in hAskMC. After confirming the transformation of hAskMC into young phenotypic characteristics (hypertrophy and myogenesis) under specific ES conditions, we proceeded to examine whether the phenotypic alteration in hAskMC is associated to senescence. Senescence-associated beta-galactosidase (SA-β-Gal) is a widely recognized cellular senescence marker that exhibits increased expression due to heightened oxidative stress and cellular damage (30, 31). The skMC undergoes senescence which not only arrests the cell cycle but also induces senescence-associated secretory phenotype (32). To determine the improvement of senescence via ES on hAskMC, SA-β-Gal staining was performed. Compared to hYskMC as a control, the number of SA-β-Gal-positive cells in hAskMC was 2.6-fold higher (Fig. 4 *A* and *B*). Notably, in hAskMC, the number of SA-β-Gal-positive cells gradually decreased with increasing ES frequency. In particular, the optimal frequency (500 Hz ES) for hypertrophy and myogenesis of hAskMC showed the lowest expression of SA-β-Gal staining. In contrast, in hYskMC, the number of SA-β-Gal-positive cells decreased at 5 and 50 Hz but significantly increased at 500 Hz. In summary, the SA-β-Gal staining results indicated that the specific ES conditions could recover the senescence-associated phenotype in hAskMC, and the optimal ES frequency minimizing the senescence marker expression was 500 Hz. In contrast, ES did not show a positive senescence-associated phenotype and led to an adverse effect at 500 Hz in the hYskMC.

To further verify the effect of ES on transcriptomic changes in the recovered senescence-associated phenotype, we examined p16, p53, and p19 mRNA levels in hYskMC and hAskMC. p16, p19, and p53 are responsible for cell cycle regulation and cellular senescence (33–35). Therefore, the expression of their corresponding genes usually increases during cell senescence (34). The results showed that the senescence-associated gene expression profiles showed a similar tendency to that shown in the SA-β-gal assay, depending on the frequencies (Fig. 4 *C*–*E*). The basal p16, p53, and p19 expression levels in hAskMC compared to those in hYskMC were 1.4-fold, 1.3-fold, and 2.1-fold higher, respectively. In contrast, when 500 Hz ES was applied to hAskMC, the expression levels of p16 and p19 significantly decreased to 57.65 and 48.4%, respectively. The p53 expression in hAskMC was the lowest at 500 Hz ES. However, in hYskMC, the gene expression profiles showed an opposite pattern to that of hAskMC. Although p16 and p19 expression levels were not changed in 5 and 50 Hz ES, they were increased 1.5-fold in the 500 Hz ES condition. The p53 expression level showed no change and a 0.5-fold decrease at 5 and 50 Hz ES in hYskMC, respectively. In contrast, at 500 Hz, it increased 2-fold. In particular, the increased expression of genes such as p16, p53, and p19 induces cell cycle arrest and cellular stress, which in turn elevates the level of reactive oxygen species (ROS) within cells. The rise in ROS levels induces DNA damage, oxidative stress, and cellular senescence (36). Therefore, we hypothesized that the decrease in the expression of p16, p53, and p19 genes due to specific ES would also result in a decrease in ROS levels. We analyzed the changes in ROS levels within cells (*SI Appendix*, Fig. S12 *A* and *B*). The results confirmed a significant increase in the basal level of ROS in hAskMC compared to hYskMC. When specific ES was applied, we observed a slight increase in ROS levels under conditions of 5 and 50 Hz in hYskMC, and a substantial increase in ROS levels was confirmed at 500 Hz, where damage occurred. On the contrary, in hAskMC, a decrease in ROS levels was observed for all stimulation conditions. Especially, this result is associated with SA-β-Gal expression, where the increase in intracellular ROS levels induces cellular senescence, thereby increasing SA-β-Gal expression. Therefore, our results reveal that applying specific ES to aged muscle cells can alleviate cellular senescence by reducing ROS levels that trigger cellular senescence. Additionally, our results demonstrate that applying a strong stimulus to hYskMC can paradoxically increase ROS levels and promote cellular senescence.

In addition, we investigated the expression levels of the inflammatory cytokine interleukin-6 (IL-6) and muscle RING-finger protein-1 (MuRF1), which show increased expression during muscle atrophy (Fig. 4 *F* and *G*) (37–39). In hAskMC, the basal IL-6 and MuRF1 levels were 2-fold and 1.4-fold higher, respectively, than those in hYskMC. However, the IL-6 expression level significantly decreased at 5 Hz by 27.5%, at 50 Hz by 33.5%, and at 500 Hz by 55%. In hYskMC, there was no significant change in IL-6 expression at 50 Hz, but at 5 Hz, IL-6 expression was decreased. However, at 500 Hz, IL-6 expression was drastically increased. Moreover, the MuRF1 expression level in the hAskMC control group was 1.4-fold higher than that in the hYskMC control group. In hAskMC, MuRF1 expression level was significantly decreased at 5 Hz by 0.5-fold (0.86-fold, 62.32%), at 50 Hz by 0.9-fold (0.52-fold, 37.68%), and at 500 Hz by 1.0-fold (0.39-fold, 28.26%) (Fig. 4*F*). In hYskMC, MuRF1 expression decreased at 5 Hz (0.22-fold, 22%) and 50 Hz (0.23-fold, 77%). However, at 500 Hz, MuRF1 expression increased 1.2-fold. Based on these results, we concluded that hAskMC can be restored closer to the hYskMC-like phenotype. In addition, we found that the 500 Hz ES condition negatively affected hYskMC. This result shows a similar tendency to that of the differentiation results. Therefore, we found that young and aged muscles can be restored or strengthened only when the appropriate ES is applied, according to age.

Enhancement of Calcium Signal and Metabolic Function in hAskMC by Specific ES. Skeletal muscle is a well-known excitable system in the human body via external stimulation. When ES is applied to skMC, the membrane potential changes, and it is recognized by the dihydropyridine receptor (DHPR), a potential receptor in the t-tubules (40). DHPR then transmits a signal to ryanodine receptor 1 (RyR1) to release calcium from the sarcoplasmic reticulum (SR) into the cytosol, and a calcium spark is generated (41–43). The released calcium binds to the troponin site on the sarcomere, which subsequently initiates muscle contraction, promotes mitochondrial energy metabolism, and induces muscle regeneration and growth (43). However, in aged muscles, calcium leakage occurs in the SR (44). Because of the calcium leak, the calcium signal is much lower in aged muscle compared with that in young muscle (45). Hence, if the calcium signal can be induced through ES, we expect that hAskMC can be more functionally recovered.

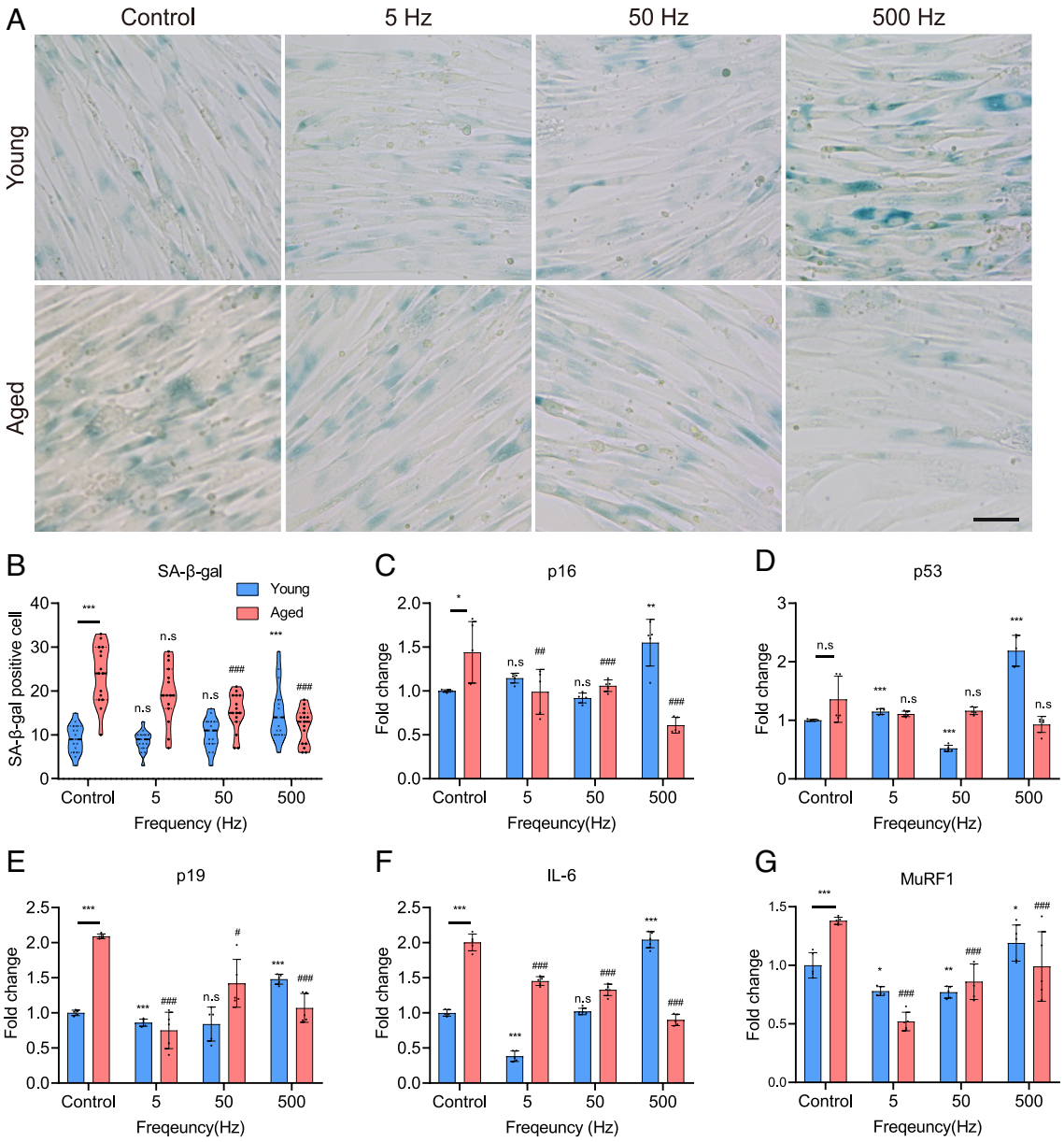

Fig. 4. Specific ES conditions reduce senescence-associated factors. (*A*) SA-β-Gal staining of hYskMC and hAskMC. Specific ES conditions that could recover the senescence-associated phenotype in the hAskMC and the optimal ES frequency for young and aged were different. (Scale bar, 50 μm.) (*B*) Quantification of SA-β-Gal-positive cells. (*C*–*G*) mRNA expression levels of p16 (*C*), p53 (*D*), p19 (*E*), IL-6 (*F*), and MuRF1 (*G*). The gene expression data elucidated that the hAskMC can be restored to the hYskMC-like phenotype. (*$P < 0.05$; **$P < 0.01$; ***$P < 0.001$; compared to young control, $^{\#}P < 0.05$; $^{\#\#}P < 0.01$; $^{\#\#\#}P < 0.001$; compared to aged control).

The calcium flux images showed that the calcium signal of hAskMC was much lower (74.1%) than that of hYskMC (Fig. 5 *A* and *B*). Interestingly, when ES was applied, the calcium flux enhancement tendency corresponded with that of myotube differentiation and senescence-associated factors. The optimal enhancement of calcium flux occurred at 50 Hz for hYskMC (1.52-fold increase) and 500 Hz for hAskMC (2.58-fold increase). In particular, while hAskMC showed a maximal calcium signal, hYskMC exhibited a minimal calcium flux (1.52-fold reduction) at 500 Hz. Subsequently, the number of calcium sparks within 5 min was quantified (Fig. 5*C*). Compared with the hYskMC control group, hAskMC showed significantly fewer sparks (74.2% reduction). However, when ES was applied to hAskMC, the number of calcium sparks was significantly increased up to 3.1-fold at 500 Hz, while it was reduced in hYskMC at the same frequency. These results suggest that the optimal ES condition is different for enhancing calcium flux depending on hYskMC and hAskMC, and the impaired calcium signal in hAskMC can be functionally recovered via specific ES conditions.

To further analyze changes in calcium signaling, we analyzed the expression levels of DHPR and RyR1 (Fig. 5 *D* and *E*). DHPR is a protein that senses the membrane potential on the t-tubule membrane and relays RyR1 to the SR. RyR1, which is located on the SR membrane, is responsible for releasing calcium ions from the SR into the cytoplasm. In hAskMC, both RyR1 and DHPR expression levels increased at 50 and 500 Hz, with the greatest increase observed in the latter condition. In hYskMC, both RyR1 and DHPR expression levels were significantly up-regulated at 50 Hz and significantly down-regulated at 500 Hz. These results showed that there was an improvement in the ES-mediated calcium signaling in hAskMC, which could potentially lead to better energy metabolism.

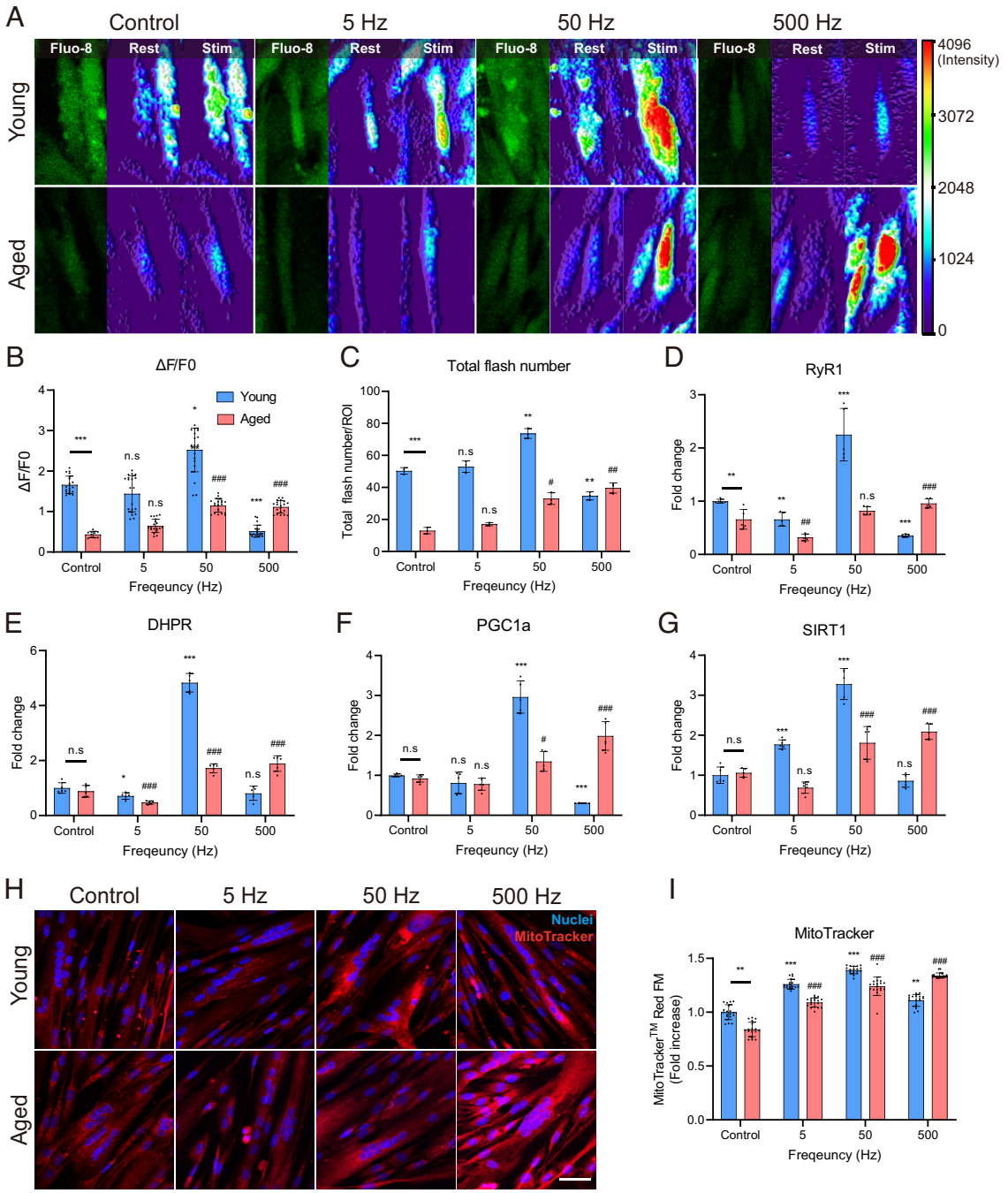

Fig. 5. Specific ES conditions lead to calcium signaling improvement and metabolic improvement in hAskMC. (*A*–*C*) Results of calcium imaging (*A*) quantification result of ΔF/F0 (*B*) and quantification result of total flash number (*C*). The optimal ES condition enhanced the calcium flux in hYskMC and hAskMC. (*D* and *E*) mRNA expression level of RyR1 (*D*) and DHPR (*E*). These results showed that there was an improvement in the specific ES-mediated calcium signaling in hAskMC. (*F* and *G*) mRNA Expression level of PGC1a (*F*) and SIRT1 (*G*). (*H* and *I*) Representation (*H*) and quantification (*I*) of MitoTracker™ Red FM staining of skMC. The specific ES condition enhances metabolic function in the hAskMC. (Scale bar, 100 μm.) (*$P < 0.05$; **$P < 0.01$; ***$P < 0.001$; compared to young control, $^{\#}P < 0.05$; $^{\#\#}P < 0.01$; $^{\#\#\#}P < 0.001$; compared to aged control).

The skeletal muscle is the most energy-consuming organ in the human body, and mitochondrial metabolism rapidly declines with aging (46). Therefore, we also analyzed the change in mitochondrial metabolic function using MitoTracker™ Red FM, whose intensity is altered by the changes in mitochondrial membrane potential. In hYskMC, 50 Hz ES showed maximal MitoTracker™ intensity (39.2% increase). In contrast, at 500 Hz, hAskMC showed the most significant improvement (60% increase) compared to the hAskMC control group (Fig. 5 *H* and *I*), which indicates that the specific ES condition enhances not only calcium flux but also metabolic function in the hAskMC.

These changes were also observed in SIRT1 and PGC1α mRNA expression levels, which induce fatty acid oxidation and mitochondria production (Fig. 5 *F* and *G*). Corresponding to the previous tendency depending on the frequency, the optimal ES conditions for PGC1α and SIRT1 expressions were also 50 and 500 Hz in hYskMC and hAskMC, respectively. In particular, 500 Hz ES resulted in maximal overexpression of the genes (2.96-fold) in hAskMC but resulted in a noticeable reduction in hYskMC. In addition, we verified whether the consistency of the metabolic function enhancement was also observed in 20M and 66M (*SI Appendix,* Fig. S13). In 20M, while there were no significant

changes in MitoTracker expression at 5 and 50 Hz, the expression of PGC1a significantly increased at 50 Hz (*SI Appendix,* Fig. S13 *A–C*). In contrast, at 500 Hz, we observed a decrease not only in MitoTracker expression but also in PGC1a expression. On the other hand, in aged cells, the expression of MitoTracker slightly increased across all frequency bands, and the expression of PGC1a and SIRT1 significantly increased as the frequency increased (*SI Appendix,* Fig. S13 *C* and *D*). These findings were consistent with those from hYskMC and hAskMC. Based on these results, it was concluded that specific ES conditions can improve calcium signaling and metabolic function in hAskMC, and the optimal ES condition differs according to the hYskMC and hAskMC. In addition, the optimal conditions for the hYskMC and hAskMC were equivalent to those effective in myotube differentiation and suppression of the aging phenotype.

Validation Study to Treat Sarcopenia via the Specific ES in Aged Mice. To verify the effect of ES, we applied ES to young (4-mo-old) and aged (24-mo-old) mice using a miniaturized electroceutical device that can generate ES conditions almost equivalent to those of the HiTESS platform (Fig. 6*A*). One of the critical challenges in this study was the translation of the in vitro ES condition into in vivo stimulation. To apply the same conditions of stimulation in the in vitro experiment, a 3D mouse leg model was created using mouse computed tomography (CT) data (Fig. 6*B*). The E-field was simulated using COMSOL, with measurements taken at the ROI where the tibialis anterior (TA) and soleus (SOL) muscles are situated. To replicate the equivalent E-field in vivo similar to the in vitro ES condition (E-field as 11.5 V/m), the simulation was performed by gradually decreasing the potential from 5 V. It was revealed that 3.7 V generated the most similar condition with the in vitro E-field, showing 11.8 V/m at the ROI (Fig. 6 *C* and *D*). We applied ES five times per week (30 min duration) for 6 wk. After completing all ES sessions, the TA and SOL muscles were isolated from the mice. To quantify the diameter of the myofibers, TA muscles were cryosectioned and stained with antibodies for laminin and Type IIA myofiber (Fig. 6*E*). The cross-sectional area (CSA) of Type IIA fiber in aged mice was significantly lower than that in young mice (Fig. 6*F*). However, when ES was applied to aged mice, the CSA increased in all conditions, with the most significant improvement resulting from 500 Hz ES (Fig. 6*G*). ES also caused significant CSA changes in young mice, with the greatest increase at 50 Hz, but the CSA drastically decreased at 500 Hz (*SI Appendix,* Fig. S14). In addition, we investigated the expression of Pax7, which plays a crucial role in muscle proliferation (47). Pax7 expression in aged mice was significantly lower than that in young mice (Fig. 6 *J* and *K*). However, when we applied a specific ES condition that showed positive effects on CSA, ES induced an increase in Pax7 expression in aged mice. In contrast, in young mice, Pax7 expression was reduced at 5 and 500 Hz. This result corresponds with the tendency observed in the in vitro experiments. Additionally, we examined the expression of proteins related to hypertrophy (Myh1/2/4/6) and atrophy (Atrogin-1) with the TA muscle of young and aged mice (*SI Appendix,* Fig. S15 *A–C*). Results showed that myosin tended to increase at 5 and 50 Hz in the young group and at 50 and 500 Hz in the aged group. Although the expression of atrogin-1, a representative protein related to atrophy, was greatly increased in the aged group compared to the young group, the ES conditions significantly reduced the expression of atrogin-1 (*SI Appendix*, Fig. S15*C*). Based on the results, we confirmed that the specific ES can induce the hypertrophy of aged skeletal muscles.

The twitch and tetanus forces were measured in the SOL muscle to evaluate the biomechanical improvement of the skeletal muscle via ES. In young mice, ES slightly improved but showed no significant change; however, it enhanced both the twitch and tetanus forces in aged mice. The optimal frequency showing maximal improvement of the forces was 500 Hz, where twitch and tetanus forces increased 1.3-fold and 1.23-fold, respectively (Fig. 6 *H* and *I* and *SI Appendix,* Fig. S15 *D and E*). In particular, it should be noted that the twitch force of aged muscles at 500 Hz ES was almost similar (97%) to that of young control muscles (Fig. 6*H*). These results clearly showed that ES enhanced the thickness of the Type IIA fiber and the contraction force in the skeletal muscle of aged mice and the optimal ES condition was 500 Hz, corresponding to the in vitro results, while the same condition caused an adverse effect in young mice. In summary, the specific ES condition induces both morphological and biomechanical improvements in aged mice, thereby confirming that the electroceutical approach has the potential to treat sarcopenia.

We then performed RNA sequencing of TA muscles from young control (n = 3), aged control (n = 3), and aged mice with 500 Hz ES (n = 3) to analyze the gene expression patterns underlying the observed increase in type II myofibers and contraction forces. The RNA sequencing data in this study have been deposited to the National Center for Biotechnology Information of the National Library of Medicine under the accession number PRJNA859543 (48). The sequencing results were analyzed using principal component analysis (PCA) to determine the statistical significance between groups (Fig. 6*L*). Fig. 6 *M* and *N* show the genes with significant differences in young vs. aged and aged ES vs. aged control. We found differentially expressed genes (DEGs) that were common between the two groups, young vs. aged and aged ES vs. aged control (Fig. 6*O*). Subsequently, we sorted the 60 genes that commonly changed between the two groups and plotted the selected genes with a heatmap (Fig. 6*P*). The results showed that while the gene expression pattern was significantly different between the young control and aged control, the gene expression profile of the aged sample subjected to 500 Hz ES shifted to the pattern closer to the young phenotype (Fig. 6*P*).

To better understand the functional improvement of skeletal muscle from the DEGs, GO analyses were performed. The results showed that six GO terms were up-regulated, including skeletal system development, response to mechanical stimulus, axon guidance, and cell differentiation, in young versus aged. In contrast, the inflammatory response and regulation of apoptosis were down-regulated (Fig. 6*Q* and *SI Appendix,* Fig. S16*A*). The results indicated that the overall muscular functions were significantly increased in the young group. In contrast, the aged control versus aged ES resulted in nine GO terms, six of which were up-regulated, including lipid metabolic process, sarcomere organization, axon guidance, proliferation regulation, myofibril assembly, and muscle structure development (Fig. 6*R* and *SI Appendix,* Fig. S16*B*). As the six GO terms play key roles in overall muscle development and integrity, ES intervention resulted in the effective recovery of the aged muscle. Furthermore, we analyzed the GO terms of young 50 and 500 Hz related to skeletal muscle myogenesis and myopathy (*SI Appendix,* Fig. S15 *F* and *G*). As a result, at 50 Hz, we found that the expression of genes related to muscle structure development, muscle cell differentiation, muscle tissue development, and other hypertrophy-related genes was increased. On the other hand, there was an increase in the expression of genes related to muscle atrophy at 500 Hz ES condition. In summary, the GO terms that are commonly changed in young and aged ES vs. aged control were skeletal muscle development, axon guidance, and proliferation regulation. Thus, the specific ES condition can restore the aged skeletal muscle

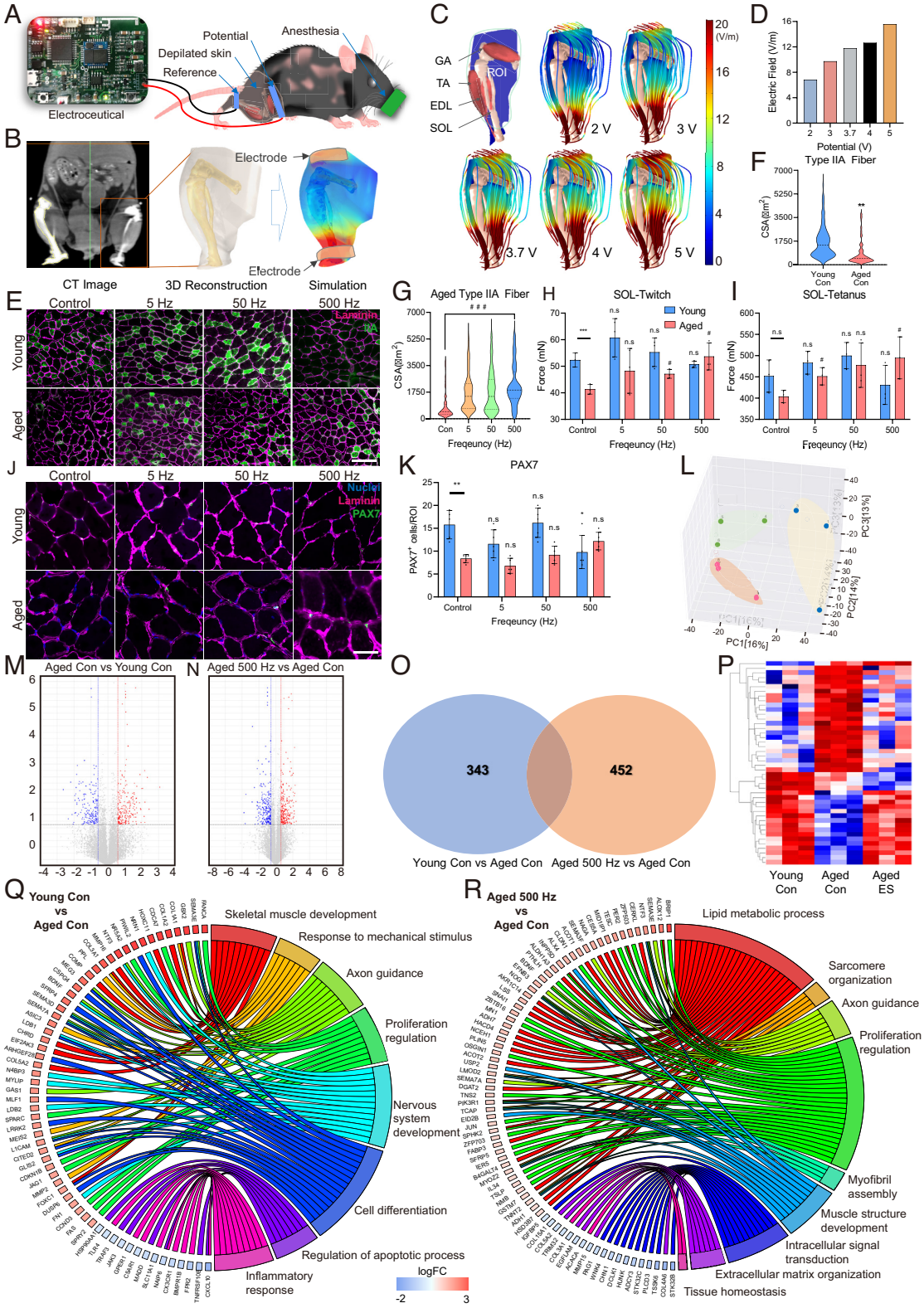

Fig. 6. Validation of the silver electroceutical in aged mice. (*A*) Schematics of the preclinical ES experiment. (*B*) E-field simulation process in a mouse leg based on 3D anatomy reconstructed by CT images. (*C*) Simulation results of E-field distribution in a mouse leg. (*D*) Quantification result of E-field value in the ROI of a mouse leg. (*E*) Representative CSA images of Type IIA muscle fibers in young and aged mice (Green; Type IIA fiber, Magenta; Laminin). (Scale bar, 200 μm.) (*F*) Quantification of myofiber CSA in young versus aged mice. (*G*) Quantification of myofiber CSA for ES conditions in aged mice. (*H* and *I*) Isometric twitch (*H*) and tetanus contraction (*I*) force measurement of soleus muscles depending on ES conditions in young and aged mice. (*J* and *K*) Representative images (Scale bar, 50 μm.) (*J*) and quantification (*K*) of the expression of PAX7 (Green) and muscle fibers (Magenta; Laminin). (*L*) Result of PCA. (*M* and *N*) Volcano plot of RNA sequencing transcriptome data displaying the pattern of gene expression values for young control (*M*) and aged 500 Hz mice (*N*) relative to aged control mice. (*O*) Venn diagram of differentially expressed genes found in aged con/young con and aged 500 Hz/young con. (*P*) Gene clustering heatmap of RNA sequencing using TA muscle from mice. (*Q* and *R*) Gene ontology analysis results for young control (*Q*) and aged 500 Hz mice (*R*) relative to aged control mice. (*$P < 0.05$; **$P < 0.01$; ***$P < 0.001$; compared to young control, $^{\#}P < 0.05$; $^{\#\#}P < 0.01$; $^{\#\#\#}P < 0.001$; compared to aged control).

phenotype closer to that of young mice. In addition, it was noted that the electroceutical approach induces not only skeletal muscle development but also nerve development.

Discussion

As sarcopenia currently lacks any FDA-approved intervention, physical exercise is the only option available to manage its symptoms. However, physical exercise is often infeasible for the aged population – the demographic most affected by sarcopenia – owing to a higher probability of falls and fractures (49). Moreover, extended COVID-19 confinement and hospitalization, which also have a higher incidence among the aged population, have accelerated sarcopenia worldwide, especially in elderly people (50). The looming risks posed by new variants of the virus have provoked repetitive lockdowns, further limiting the opportunities for physical exercise. Owing to these adverse circumstances, a feasible treatment for sarcopenia with minimal side effects is urgently required.

To ascertain the potential for treating sarcopenia using electroceutical approach, it is essential to conduct experiments with minimal cells, as valuable human aged skMCs need to be utilized. Moreover, it is crucial to be able to simultaneously apply various ES conditions to cells within a precise and uniform E-field environment. Previous studies on ES primarily utilized skeletal muscle cell lines derived from rodents, which do not accurately reflect the characteristics of aged human skMCs (17, 51). These studies were limited by employing batch-type systems that only allowed for a few ES conditions to be applied, making it difficult to explore optimal ES conditions (combinations of voltage, frequency, and duration) (23). Additionally, they resulted in nonuniform E-field distribution on the cells and required a substantial number of cells for experiments (52). Furthermore, ES platform needs to be also considered for joule heating, which poses potential risks for cell damage. In contrast, the HiTESS platform satisfies the multiple requirements, including HiTESSs, uniform E-field distribution, utilization of a minimal number of cells, and decoupled joule heating.

Homeostasis of calcium signaling plays a crucial role in maintaining healthy skeletal muscle function. During sarcopenia, calcium leak occurs from the SR, and the released calcium increases ROS or RNS levels, causing muscle damage (44). At the same time, it has been well known that as skeletal muscle ages, the calcium influx deteriorates due to denervation, leading to mitochondrial dysfunction and elevated ROS levels (44, 53). Ultimately, since homeostasis in calcium signaling is disrupted in aged skeletal muscle, recovering calcium signaling is crucial to improve the functions of skeletal muscles (54). The clinical trial to improve the calcium signal as a small molecule is one of the representative examples to emphasize the need for sarcopenia treatment (55).

Our major hypothesis was if specific ES can restore calcium signaling in aged skeletal muscles, inducing hypertrophy. Since there are few reports to show the potential that ES can induce hypertrophy in hAskMC, we first investigated the optimal ES condition to induce hypertrophy of hAskMC with the HiTESS platform, finally identifying the maximal hypertrophy condition as 500 Hz ES. Interestingly, the specific ES not only significantly increased the calcium influx as well as mitochondrial function but alleviated ROS level in the hAskMC. It was presumed that the increase of the calcium influx via the specific ES is responsible for the DHPR, normally a voltage-dependent calcium channel functioning essentially as a voltage sensor in skeletal muscle (56). During the aging process of skeletal muscles, the density of T-tubules decreases, reducing the distribution of DHPR (53, 57). However, our data exhibited that the specific ES significantly induced both mRNA expressions of DHPR and RyR1. This considerable increase might lead to enhanced response to external stimuli such as ES in aged skeletal muscles (*SI Appendix*, Fig. S17). The different expressions of DHPR depending on young and aged skeletal muscles (53), might be one of the major reasons that the skMCs responded to ES conditions differently at age.

One of the key factors contributing to the age-related decline of skeletal muscles is the decrease in neuromuscular junction (NMJ) density. As aging occurs, the NMJ undergoes fragmentation, denervation, and a reduced synaptic contact area between motor neurons and muscle fibers (58, 59). Denervation is known to exacerbate muscle fiber (primarily type II) loss and lower CSA (60, 61). This suggest that the enhancement of skeletal muscle alone might not be the fundamental solution to treat sarcopenia, as it may ultimately induce muscle atrophy again. Therefore, to treat sarcopenia, it is more desirable to improve not only the skeletal muscles but also the motor nerves. The RNA sequencing results showed that the optimal ES induced not only the development and differentiation of skeletal muscles but also neurogenesis in the aged ES group. In addition, our previous research shows that an electroceutical approach can be an alternative to treating Charcot-Marie-Tooth by improving myelination (62, 63). Therefore, the electroceutical approach has a unique advantage over biochemical approaches that showed improvements in the skeletal muscles alone.

Electroceutical treatment for sarcopenia has good prospects for clinical application. Recently, excellent progress has been achieved toward developing implantable miniature wireless ES devices (64). Furthermore, the development of soft and electroactive biomaterials has reduced the physical mismatch at the tissue-device boundary (65), thereby making long-term electroceutical treatment more viable. It should be noted that ES devices have been considerably developed toward neuromodulation, and skeletal muscle stimulation has received relatively less attention. Currently, many electrical muscle stimulation devices have been used in hospitals and homes without considering the optimal ES conditions. Through this research, we suggest that a specific ES for sarcopenia needs to be applied to maximize the effect with minimal side effects, and we wish to call the introduced technology silver electroceutical. In addition, it is crucial to consider specific ES conditions depending on age to maximize the efficacy of the intervention. This study can potentially be the basis for the development of personalized bioelectric medicine for sarcopenia.

Materials and Methods

The materials and methods are described in detail in *SI Appendix, Material and Methods*, including simulation for optimizing the electric field uniformity of the HiTESS chip, construction of the HiTESS platform, analysis of Lipofuscin and ROS expression using fluorescence-activated cell sorting, cultivation of human-derived primary skeletal muscle cell and electrical stimulation, cryosection and immunostaining, senescence-associated β-galactosidase (SA-β-Gal) assay, metabolic ability evaluation through MitoTracker™ Red FM staining, calcium imaging, real-time PCR, simulation for in vivo electrical stimulation and ES intervention process, isometric contractile force analysis, gene ontology analysis through RNA sequencing, and western blot analysis.

Statistical Analyses. Statistical analyses were performed using GraphPad Prism version 8. All data are presented as mean ± SD, as indicated in the figure legends. Statistical significance was calculated using *t* test (two groups) and one-way ANOVA (over two groups), and expressed as follows: *, #$P < 0.05$, **, ##$P < 0.01$,

***, ###$P < 0.001$. Differences were considered to be statistically significant at $P \leq 0.05$.

Data, Materials, and Software Availability. RNA seq data have been deposited in the NIH SRA (PRJNA859543) (48). All study data are included in the article and/or *SI Appendix*.

ACKNOWLEDGMENTS. This work was supported by the National Research Foundation of Korea funded by the Korea government (No. 2022R1A2C209187012).

Author affiliations: [a]Department of New Biology, Daegu Gyeongbuk Institute of Science and Technology, Daegu 42988, Republic of Korea; [b]CTCELLS, Inc., Daegu 42988, Republic of Korea; [c]SBCure Corp., Daegu 43017, Republic of Korea; [d]Well Aging Research Center, Daegu Gyeongbuk Institute of Science and Technology, Daegu 42988, Republic of Korea; [e]Samsung Advanced Institute of Technology, Samsung Electronics Co. Ltd., Suwon 16678, Republic of Korea; [f]Department of Molecular Cell Biology, Sungkyunkwan University School of Medicine, Suwon 16419, Republic of Korea; [g]Chonnam National University Medical School, Gwangju 61186, Republic of Korea; [h]Gene Expression Laboratory, Salk Institute for Biological Studies, La Jolla, CA 92037; [i]Translational Responsive Medicine Center, Daegu Gyeongbuk Institute of Science and Technology, Daegu 42988, Republic of Korea; and [j]New Biology Research Center, Daegu Gyeongbuk Institute of Science and Technology, Daegu 42988, Republic of Korea

1. J. D. Walston, Sarcopenia in older adults. *Curr. Opin. Rheumatol.* **24**, 623–627 (2012).
2. A. J. Cruz-Jentoft, A. A. Sayer, Sarcopenia. *Lancet* **393**, 2636–2646 (2019).
3. E. Marty, Y. Liu, A. Samuel, O. Or, J. Lane, A review of sarcopenia: Enhancing awareness of an increasingly prevalent disease. *Bone* **105**, 276–286 (2017).
4. Y. Feike, L. Zhijie, C. Wei, Advances in research on pharmacotherapy of sarcopenia. *Aging Med. (Milton)* **4**, 221–233 (2021).
5. G. Parise, T. Snijders, Myostatin inhibition for treatment of sarcopenia. *Lancet Diabetes Endocrinol.* **3**, 917–918 (2015).
6. J. Suh, Y. S. Lee, Myostatin inhibitors: Panacea or predicament for musculoskeletal disorders? *J. Bone Metab.* **27**, 151–165 (2020).
7. C. Vinel *et al.*, The exerkine apelin reverses age-associated sarcopenia. *Nat. Med.* **24**, 1360–1371 (2018).
8. M. G. Hanna *et al.*, Safety and efficacy of intravenous bimagrumab in inclusion body myositis (RESILIENT): A randomised, double-blind, placebo-controlled phase 2b trial. *Lancet Neurol.* **18**, 834–844 (2019).
9. T. L. Nielsen, J. Vissing, T. O. Krag, Antimyostatin treatment in health and disease: The story of great expectations and limited success. *Cells* **10**, 533 (2021).
10. R. M. Helge Amthor *et al.*, Lack of myostatin results in excessive muscle growth but impaired force generation. *Proc. Natl. Acad. Sci. U.S.A.* **104**, 1835–1840 (2017).
11. J. E. Morley, Treatment of sarcopenia: The road to the future. *J. Cachexia Sarcopenia Muscle* **9**, 1196–1199 (2018).
12. F. Landi, E. Marzetti, A. M. Martone, R. Bernabei, G. Onder, Exercise as a remedy for sarcopenia. *Curr. Opin. Clin. Nutr. Metab. Care* **17**, 25–31 (2014).
13. C. Julio Benvenutti Bueno de *et al.*, Inactivity during COVID-19 quarantine and its effects in strength and functional parameters in elderly: A case-study. *Int. J. Sport Exerc. Health Res.* **6**, 180 (2020).
14. W. K. Abdelbasset, Stay home: Role of physical exercise training in elderly individuals' ability to face the COVID-19 infection. *J. Immunol. Res.* **2020**, 8375096 (2020).
15. J. Y. Kwak, K.-S. Kwon, Pharmacological interventions for treatment of sarcopenia: Current status of drug development for sarcopenia. *Ann. Geriatr. Med. Res.* **23**, 98–104 (2019).
16. L. Campins *et al.*, Oral drugs related with muscle wasting and sarcopenia. A review. *Pharmacology* **99**, 1–8 (2017).
17. N. Nikolic *et al.*, Electrical pulse stimulation of cultured skeletal muscle cells as a model for in vitro exercise - possibilities and limitations. *Acta Physiol. (Oxf)* **220**, 310–331 (2017).
18. K. Danilov *et al.*, Electrical pulse stimulation decreases electrochemical Na(+) and K(+) gradients in C2C12 myotubes. *Biochem. Biophys. Res. Commun.* **493**, 875–878 (2017).
19. M. M. Nishida, T. Tsuboyama, T. Moritani, H. Arai, Review of the evidence on the use of electrical muscle stimulation to treat sarcopenia. *European Geriatr. Med.* **7**, 267–271 (2016).
20. K. Ikeda, A. Ito, M. Sato, Y. Kawabe, M. Kamihira, Improved contractile force generation of tissue-engineered skeletal muscle constructs by IGF-I and Bcl-2 gene transfer with electrical pulse stimulation. *Regen. Ther.* **3**, 38–44 (2016).
21. S. Bayol, C. Brownson, P. T. Loughna, Electrical stimulation modulates IGF binding protein transcript levels in C2C12 myotubes. *Cell Biochem. Funct.* **23**, 361–365 (2005).
22. Y. Kawahara *et al.*, Novel electrical stimulation sets the cultured myoblast contractile function to "on". *Pathobiology* **73**, 288–294 (2006).
23. H. Park *et al.*, Effects of electrical stimulation in C2C12 muscle constructs. *J. Tissue Eng. Regen. Med.* **2**, 279–287 (2008).
24. V. Eisner, V. Parra, S. Lavandero, C. Hidalgo, E. Jaimovich, Mitochondria fine-tune the slow Ca(2+) transients induced by electrical stimulation of skeletal myotubes. *Cell Calcium* **48**, 358–370 (2010).
25. B. T. Zhang *et al.*, The effects of low frequency electrical stimulation on satellite cell activity in rat skeletal muscle during hindlimb suspension. *BMC Cell Biol.* **11**, 87 (2010).
26. H. Fujiya *et al.*, Microcurrent electrical neuromuscular stimulation facilitates regeneration of injured skeletal muscle in mice. *J. Sports Sci. Med.* **14**, 297–303 (2015).
27. G. M. Xiong *et al.*, Development of a miniaturized stimulation device for electrical stimulation of cells. *J. Biol. Eng.* **9**, 14 (2015).
28. H. Y. Shin *et al.*, Cell seeding technology for microarray-based quantitative human primary skeletal muscle cell analysis. *Anal. Chem.* **91**, 14214–14219 (2019).
29. C. C. Agley, C. P. Velloso, N. R. Lazarus, S. D. Harridge, An image analysis method for the precise selection and quantitation of fluorescently labeled cellular constituents: Application to the measurement of human muscle cells in culture. *J. Histochem. Cytochem.* **60**, 428–438 (2012).
30. C. Cazin, A. Chiche, H. Li, Evaluation of injury-induced senescence and in vivo reprogramming in the skeletal muscle. *J. Vis. Exp.* **26**, 56201 (2017).
31. F. Debacq-Chainiaux, J. D. Erusalimsky, J. Campisi, O. Toussaint, Protocols to detect senescence-associated beta-galactosidase (SA-betagal) activity, a biomarker of senescent cells in culture and in vivo. *Nat. Protoc* **4**, 1798–1806 (2009).
32. M. Wan, E. F. Gray-Gaillard, J. H. Elisseeff, Cellular senescence in musculoskeletal homeostasis, diseases, and regeneration. *Bone Res.* **9**, 41 (2021).
33. A. Rufini, P. Tucci, I. Celardo, G. Melino, Senescence and aging: The critical roles of p53. *Oncogene* **32**, 5129–5143 (2013).
34. S. Mankhong *et al.*, Experimental models of sarcopenia: Bridging molecular mechanism and therapeutic strategy. *Cells* **9**, 1385 (2020).
35. H. Sugihara *et al.*, Cellular senescence-mediated exacerbation of duchenne muscular dystrophy. *Sci. Rep.* **10**, 16385 (2020).
36. Y. C. Jang *et al.*, Increased superoxide in vivo accelerates age-associated muscle atrophy through mitochondrial dysfunction and neuromuscular junction degeneration. *FASEB J.* **24**, 1376–1390 (2010).
37. I. W. McKinnell, M. A. Rudnicki, Molecular mechanisms of muscle atrophy. *Cell* **119**, 907–910 (2004).
38. C. Nylen *et al.*, IL6 and LIF mRNA expression in skeletal muscle is regulated by AMPK and the transcription factors NFYC, ZBTB14, and SP1. *Am. J. Physiol. Endocrinol. Metab.* **315**, 995–1004 (2018).
39. Y. D. Rong, A. L. Bian, H. Y. Hu, Y. Ma, X. Z. Zhou, Study on relationship between elderly sarcopenia and inflammatory cytokine IL-6, anti-inflammatory cytokine IL-10. *BMC Geriatr.* **18**, 308 (2018).
40. C. Franzini-Armstrong, A. G. Engel, "Skeletal muscle: Architecture of membrane systems" in *Muscle*, J. A. Hill, E. N. Olson, Eds. (Elsevier Inc., Netherlands, 2012). **vol. 53**, pp. 763–774, 10.1016/b978-0-12-381510-1.00054-5 chap.
41. M. Casas *et al.*, IP(3)-dependent, post-tetanic calcium transients induced by electrostimulation of adult skeletal muscle fibers. *J. Gen. Physiol.* **136**, 455–467 (2010).
42. C. R. Lamboley, V. L. Wyckelsma, M. J. McKenna, R. M. Murphy, G. D. Lamb, Ca(2+) leakage out of the sarcoplasmic reticulum is increased in type I skeletal muscle fibres in aged humans. *J. Physiol.* **594**, 469–481 (2016).
43. M. K. Tu, J. B. Levin, A. M. Hamilton, L. N. Borodinsky, Calcium signaling in skeletal muscle development, maintenance and regeneration. *Cell Calcium* **59**, 91–97 (2016).
44. D. C. Andersson *et al.*, Ryanodine receptor oxidation causes intracellular calcium leak and muscle weakness in aging. *Cell Metab.* **14**, 196–207 (2011).
45. K. H. Park *et al.*, Assessment of calcium sparks in intact skeletal muscle fibers. *J. Vis. Exp.* **24**, e50898 (2014), 10.3791/50898.
46. E. Rezus *et al.*, Inactivity and skeletal muscle metabolism: A vicious cycle in old age. *Int. J. Mol. Sci.* **21**, 592 (2020).
47. C. Lepper, S. J. Conway, C. M. Fan, Adult satellite cells and embryonic muscle progenitors have distinct genetic requirements. *Nature* **460**, 627–631 (2009).
48. M. Y. Kim, M. S. Kim, Silver Electroceutical Technology to Treat Sarcopenia. National Library of Medicine. https://dataview.ncbi.nlm.nih.gov/object/PRJNA859543?reviewer=v6ij9f55phvti8chpuvdtu80gn. Accessed 18 July 2022.
49. R. Kirwan *et al.*, Sarcopenia during COVID-19 lockdown restrictions: Long-term health effects of short-term muscle loss. *Geroscience* **42**, 1547–1578 (2020).
50. S. S. Y. Yeung *et al.*, Sarcopenia and its association with falls and fractures in older adults: A systematic review and meta-analysis. *J. Cachexia Sarcopenia Muscle* **10**, 485–500 (2019).
51. M. P. Willand *et al.*, Electrical muscle stimulation elevates intramuscular BDNF and GDNF mRNA following peripheral nerve injury and repair in rats. *Neuroscience* **334**, 93–104 (2016).
52. N. Nikolic *et al.*, Electrical pulse stimulation of cultured human skeletal muscle cells as an in vitro model of exercise. *PLoS One* **7**, e33203 (2012).
53. C. H. T. Kong *et al.*, The effects of aging on the regulation of T-tubular ICa by caveolin in mouse ventricular *Myocytes*. *J. Gerontol. A Biol. Sci. Med. Sci.* **73**, 711–719 (2018).
54. S. Schiaffino, C. Reggiani, Fiber types in mammalian skeletal muscles. *Physiol. Rev.* **91**, 1447–1531 (2011).
55. A. Ogonowska-Slodownik *et al.*, Aquatic therapy for persons with neuromuscular diseases–A scoping review. *J. Neuromuscul. Dis.* **9**, 237–256 (2022).
56. V. Schartner *et al.*, Dihydropyridine receptor (DHPR, CACNA1S) congenital myopathy. *Acta Neuropathol.* **133**, 517–533 (2017).
57. O. D. M. R. M. L. Messi, Regulation of mouse skeletal muscle L-type Ca2 channel by activation of the insulin-like growth factor-1 receptor. *J. Neurosci.* **17**, 6918–6928.
58. A. S. Arnold *et al.*, Morphological and functional remodelling of the neuromuscular junction by skeletal muscle PGC-1alpha. *Nat. Commun.* **5**, 3569 (2014).
59. Y. C. Jang, H. Van Remmen, Age-associated alterations of the neuromuscular junction. *Exp. Gerontol.* **46**, 193–198 (2011).
60. R. R. Kalyani, M. Corriere, L. Ferrucci, Age-related and disease-related muscle loss: The effect of diabetes, obesity, and other diseases. *Lancet Diabetes Endocrinol.* **2**, 819–829 (2014).
61. R. Nilwik *et al.*, The decline in skeletal muscle mass with aging is mainly attributed to a reduction in type II muscle fiber size. *Exp. Gerontol.* **48**, 492–498 (2013).
62. A. Intisar *et al.*, An electroceutical approach enhances myelination via upregulation of lipid biosynthesis in the dorsal root ganglion. *Biofabrication* **14**, 015017 (2022).
63. A. Intisar *et al.*, Implantable electroceutical approach improves myelination by restoring membrane integrity in a mouse model of peripheral demyelinating neuropathy. *Adv. Sci.* **9**, e2201358 (2022), 10.1002/advs.202201358.
64. A. Singer, J. T. Robinson, Wireless power delivery techniques for miniature implantable bioelectronics. *Adv. Healthc. Mater.* **10**, e2100664 (2021).
65. Y. Zhou *et al.*, Implantable thin film devices as brain-computer interfaces: Recent advances in design and fabrication approaches. *Coatings* **11**, 204 (2021).